


RESEARCH

Open Access



Circ_0001947 encapsulated by small extracellular vesicles promotes gastric cancer progression and anti-PD-1 resistance by modulating CD8⁺ T cell exhaustion

Bingyu Wang^{1†}, Wenbo Liu^{1†}, Mingming Zhang², Yong Li¹, Hongyue Tang², Yingying Wang¹, Chao Song¹, Buyun Song¹ and Bibo Tan^{1*} 

Abstract

Background While small extracellular vesicles (sEVs)-derived circular RNAs (circRNAs) have been emerged as significant players in cancer, the function and underlying mechanism of sEVs-derived circRNAs in anti-cancer immunity remain unclear.

Methods Gastric cancer (GC)-derived circRNAs were identified using RNA-seq data from GEO datasets and quantitative reverse transcription polymerase chain reaction (qRT-PCR), RNA immunoprecipitation, dual-luciferase assay, and bioinformatics analysis were performed to investigate the regulatory axis. Transwell assay, wound healing assay, cell counting kit-8 (CCK-8) assay, and xenograft models were used to evaluate its role in GC progression in vivo and in vitro. The delivery of specific circRNAs into sEVs were verified through electron microscopy, nanoparticle tracking analysis (NTA) and fluorescence in situ hybridization (FISH). Flow cytometric analysis and immunohistochemical staining were conducted to find out how specific circRNAs mediated CD8⁺T cell exhaustion and resistant to anti-programmed cell death 1 (PD-1) therapy.

Results We identified that circ_0001947, packaged by GC-derived sEVs, was obviously elevated in GC and was associated with poor clinical outcome. High circ0001947 level augmented the proliferation, migration, and invasion of GC cells. Mechanistically, circ0001947 sponged miR-661 and miR-671-5p to promote the expression of CD39, which further facilitated CD8⁺T cell exhaustion and immune resistance. Conversely, blocking circ_0001947 attenuated CD8⁺T cell exhaustion and increased the response to anti-PD-1 therapy.

Conclusions Our study manifested the therapeutic potential of targeting sEVs-transmitted circ_0001947 to prohibit CD8⁺T cell exhaustion and immune resistance in GC.

Keywords Tumor microenvironment, Circular RNAs, CD8⁺T cell exhaustion, Immune resistance, Small extracellular vesicles

[†]Bingyu Wang and Wenbo Liu contributed equally to this work.

*Correspondence:

Bibo Tan
tanbibo@hebmu.edu.cn

¹The Third Department of Surgery, The Fourth Hospital of Hebei Medical University, Shijiazhuang 050011, China

²Hebei Key Laboratory of Metabolic Disease, Shijiazhuang 050011, China



Introduction

Gastric cancer (GC) is one of the most prevalent malignancies and the top three causes of cancer-related mortality globally [1]. Although GC diagnosis and therapy have achieved advancements, the prognosis of patients remains unsatisfactory. Immune checkpoint blockade (ICB) that targets PD-1, PD-L1, and CTLA-4 has made great success in reversing immunosuppression in anti-cancer therapy [2], and anti-PD-1 therapy has become the first-line therapeutic strategy for patients with unresectable or metastatic GC [3, 4], which has been verified to effectively prolong the 5-year overall survival. Although the promising immunotherapy has shed a light on future directions, most GC patients failed to respond to checkpoint therapy [5, 6]. Therefore, strategies for overcoming the immune resistance to anti-PD-1 therapy are urgently needed.

The tumor microenvironment (TME) is a pivotal precondition for the response to ICB [7]. As an important courier in the TME, sEVs, the 30-150nm membrane-enclosed particles derived from various cell types [8], contribute to the cancer-stroma crosstalk through transferring abundant bioactive molecules [9], which furthermore make sEVs candidate treatment targets. Accumulating research has demonstrated that sEVs contained multiple signals including proteins, non-coding RNAs, and lipids to reshape the TME and engaged in immune escape and tumor progression [10–12]. CircRNAs are a type of non-coding RNAs that are highly stable due to their covalent loop structures without 5' caps, 3' tails [13]. Mechanistically, circRNAs exert their regulatory effects on GC mainly by functioning as microRNAs (miRNAs) sponges to mediate the downstream expression [14, 15]. Furthermore, it has been manifested that circRNAs could be transmitted into sEVs to involve in diverse processes such as tumor occurrence, and drug resistance [16, 17], implying that TME may be influenced by sEVs-delivered circRNAs. As the major effector cells in the process of anti-cancer immunity, the number and cytotoxic ability of CD8⁺ T cells largely determine the immunotherapy outcomes [18–20]. Under some circumstances, CD8⁺ T cells gradually display weakened proliferative capacity and reduced cytotoxic molecules, which is referred to as “CD8⁺ T cells exhaustion” [21]. Exhausted CD8⁺ T cells are characterized by upregulated level of inhibitory molecules such as PD-1 and T cell immunoglobulin domain and mucin domain 3 (Tim-3) and downregulated level of cytotoxic molecules such as interferon (IFN)- γ , granzyme B (GZMB), and perforin [22]. CD39 (ENTPD1) is a ectoenzyme that hydrolyze adenosine triphosphate (ATP) and has been proven to skew CD8⁺ T cells toward exhaustion phenotype [23, 24]. However, the complex relationship between

sEVs-derived circRNAs and the status of CD8⁺ T cells in GC is still unknown.

In this study, we identified that circ_0001947 (circAFF2) was significantly upregulated in GC-derived sEVs and was correlated with GC cells proliferation, invasion, and migration and worse prognosis in GC patients. More importantly, circ_0001947 encapsulated by sEVs contributed to CD8⁺ T cells exhaustion, resulting in the resistance to anti-PD-1 therapy. Mechanistically, circ_0001947 served as a sponge of miR-661 and miR-671-5p to augment CD39 expression, which ultimately promoting cancer progression and immune resistance. Thus, our results suggested that sEVs-transmitted circ_0001947 is a potential target for reversing CD8⁺ T cells exhaustion in GC and improving the response to ICB.

Methods

Cell lines

The human gastric epithelial cell line GES-1, human GC cell line AGS, and murine GC cell line MFC were purchased from the National Infrastructure of Cell Line Resource (NICR, China). All cells were cultured in DMEM (Gibco, USA) supplemented with 10% fetal bovine serum (FBS; Gibco, USA), 100 U/ml penicillin and 100 μ g/ml streptomycin in a humidified incubator with 5% CO₂.

Human tissue samples

A total of 30 pairs of GC tissues and adjacent normal tissues were collected from patients who were diagnosed with GC and underwent surgery at the Fourth Affiliated Hospital of Hebei Medical University from 2017 to 2022. All samples were obtained with informed content and preserved in lipid nitrogen for further use. Two experts confirmed histological and pathological diagnosis and performed according to the International Ethical Guidelines for Biomedical Research Involving Human Subjects. All related procedures were conducted with the approval of the internal review and ethics boards of the Fourth Affiliated Hospital of Hebei Medical University (approval number 2019ME0039).

sEVs isolation and identification

Cells cultured in 10% vesicle-depleted medium without FBS were prepared for sEVs extraction. Conditioned medium (CM) was collected after 48h incubation and centrifuged at 300 x g for 5 min, followed by 3000 x g for 15 min to remove all cell debris and apoptotic vesicles. CM was then purified through a 0.22 μ m filter (Millipore, USA), followed by ultracentrifugation spins at 100 000 x g for 70 min at 4 °C to pellet sEVs. Purified sEVs were collected through washing pellet with PBS and centrifuging at 100 000 x g for 70 min at 4 °C. Finally, sEVs were

resuspended in PBS and remaining pellet was reconstituted and deposited at -80°C .

Transmission electron microscope (JEOL, Japan) was applied to identify the morphology of sEVs. Identification of sEVs protein markers was conducted by Western blot. The sEVs concentration and size were measured using a nanoparticle tracking analysis (NTA) with NanoSight N300 (Malvern, UK) and analyzed with NTA analytical software version 3.4.

sEVs uptake experiment

sEVs purified from GC cells were co-cultured with PKH-26 red fluorescent Cell Linker Mini Kit (Sigma-Aldrich, USA) at room temperature for 5 min. $\text{CD8}^+\text{T}$ cells were cultured in laser confocal culture dishes and co-cultured with PKH26-labeled sEVs for 24h. Then the nuclei of $\text{CD8}^+\text{T}$ cells was colored with 4,6-diamidino-2-phenylindole (DAPI) for 10 min, and the staining was observed with fluorescence microscope (Olympus FV3000, Japan).

FISH assay

FISH was conducted according to manufacturer's constructions as previously described [25]. GC cells were cultured in confocal dishes and fixed with 4% paraformaldehyde for 25 min. Then, cells with Cy3-labeled circ_0001947 probe (GenePharma, China) were hybridized at 37°C overnight. DAPI was used for counterstaining the cell nuclei. After that, the images of circ_0001947 subcellular distribution were captured under a ZEISS LSM800 confocal microscope (Carl Zeiss AG, Germany).

RNase R treatment and actinomycin D assay

For RNase R treatment, 2 μg of total RNA extracted from AGS cells was incubated with RNase R (Epicenter Technologies, USA) for 30 min at 37°C to degrade liner RNA. The stability of circAFF2 and AFF2 mRNA was tested by qRT-PCR.

For Actinomycin D assay, after 24h incubation of AGS cells in 6-well plate, 2 mg/l actinomycin D (Sigma, USA) was added into each well for 4, 8, 12, 16h respectively. Then the cells were collected at the indicated time points for qRT-PCR.

RNA extraction and qRT-PCR

Total RNA was extracted using TRIzol reagent (Invitrogen, USA) according to the manufacturer's recommendations. cDNA was reverse described with a PrimeScriptTM RT Reagent Kit (TaKaRa, Japan). qRT-PCR was carried out through QuantstudioTM DX system (Applied Biosystems, Singapore). β -actin was used as internal control. Relative expressions were calculated by using $2^{-\Delta\Delta\text{CT}}$ method.

Plasmid construction and cell transfection

To construct the circ_00001947, circ_0004592 and circ_0077736 knockdown plasmid, small hairpin RNAs (shRNAs) targeting the junction region of related circRNAs were synthesized and cloned into the pGPU6/GFP/puromycin vector (IGE Biotech Co, China). GC cells were transfected with plasmids following the manufacturer's instructions according to previous research [26]. The miR-661 mimics, miR-671-5p mimics, miR-661 inhibitors, and miR-671-5p inhibitors were purchased from GenePharma Company (Shanghai, China) and Lipofectamine RNAiMAX (Invitrogen, USA) was used for transfection.

Dual-luciferase assay

The wild-type (WT) and mutant (MT) circ_0001947 were recombined into psiCHECK-2 (Promega, USA) for the luciferase assay. 4×10^4 HEK293 cells per well were plated into 24-well plates overnight and co-transfected with a WT vector or MT vector and miRNA mimics or control mimics with Lipofectamine 2000. After 48h co-transfection, the luciferase activity was detected using dual-luciferase reporter assay system (Promega, USA).

CCK-8 assay

CCK-8 assay was performed to assess the proliferation ability of GC cells. AGS cells were planted on 96-well plates at a density of 2×10^3 per well, then 20 μl CCK-8 solutions was added into each well at the indicated point of 24, 48, and 72h of culture. Finally, the optical density (OD) was measured at 450 nm.

Cell migration and invasion assays

For transwell assay, cells were seeded into a BD Transwell chamber (CoStar, USA) with 24 wells. After 24h, the cells across the membrane were fixed with 4% formaldehyde and stained by 0.2% crystal violet for 20 min to identify the migrated and invaded cells. The stained cells were calculated in three random fields.

For wound healing assay, cells were cultured in a 6-well plated at a density of 2×10^4 per well and scraped using 1000 ml pipette tips. The artificial wounds were detected at 0 and 24h after scratch.

CD8⁺T cell isolation

10 ml fresh peripheral blood were collected from healthy donors and human $\text{CD8}^+\text{T}$ cells were isolated and purified peripheral blood mononuclear cells (PBMCs) by an Easy-SepTM Direct Human $\text{CD8}^+\text{T}$ Cell Isolation Kit (STEMCELL Technologies, Canada). Afterwards, $\text{CD8}^+\text{T}$ cells were plated into 24-well plates and incubated with anti-CD3/anti-CD28 antibodies (R&D Systems, USA) at 2 μl /well and IL2 (Abcam, UK) at 20 ng/ml for 48h to activate.

sEVs incubation with CD8⁺T cell

sEVs (500 µg) derived from GC cells were seeded into 12-well plates and preactivated CD8⁺T cells were added. CD8⁺T cells were analyzed by using flow cytometry after 24h incubation.

Flow cytometry

Isolated cells from PBMCs were processed into single-cell suspensions and incubated with surface markers for 20 min, on ice in the dark. Then BD Cytofix Kit (BD Biosciences, USA) was used for stain intracellular markers according to the manufacturer's instructions. The expressions were detected using BD Accuri C6 flow cytometer (BD Biosciences, USA). The following surface and intracellular markers were used: CD3 (BD Biosciences, 341091), CD45 (BD Biosciences, 348795), CD8 (BD Biosciences, 341051), PD-1 (BD Biosciences, 570479), Tim-3 (BD Biosciences, 567124), IFN-γ (BD Biosciences, 569266), perforin (BD Biosciences, 563762), and Granzyme B (BD Biosciences, 571118).

RIP assay

The RIP assay was conducted using the RNA-binding protein immunoprecipitation kit (Millipore, USA) following the manufacturer's protocols as previously described [26]. GC cells were harvested and lysed in RIP lysis buffer. Cell lysates were incubated with protein A/G agarose beads (Roche, USA) conjugated with anti-AGO2 (CST, #2897S) or anti-IgG (CST, #7074S) antibody overnight at 4 °C, then washed with wash buffer. The beads-bound RNAs were purified and the enrichment values of circ_0001947 were detected by qRT-PCR.

Western blot analysis

Proteins extracted from cells were separated by SDS-polyacrylamide gels and transferred onto PVDF membranes. The following primary antibodies against CD63 (Abcam, ab193349), CD81 (Abcam, ab79559), TSG101 (Abcam, ab133586), Calnexin (Abcam, ab112995), CD39 (Abcam, ab223842), β-actin (Abcam, ab8227) were used. Then the blots were incubated with secondary antibodies for 2h at room temperature and the signals were visualized via enhanced chemiluminescence assay (ECL) (Thermo Fisher, USA).

Animal models

All animal experiments were approved by the Committee on the Ethics of Animal Experiments of Hebei Medical University. 4–6 weeks old 615 mice were purchased from Institute of Hematology & Blood Disease Hospital, Chinese Academy of Medical Science (Tianjin, China) and MFC cell line transfected with circ_001947 shRNA and control vector was prepared for animal experiment. First, all mice were divided randomly into the knockdown

control group (sh-NC group) and circ_0001947 knock-down group (sh-circ_001947 group) ($n=5$) to evaluate the function of circ_001947 on gastric cancer. A total of 2×10^6 MFC cells were inoculated into the right side of mice. Next, to explore the impact of sEVs-transmitted circ_0001947 on CD8⁺T cell exhaustion, the mice were divided into four groups ($n=5$) including the knock-down-control sEVs group treated with 0.9% normal saline (NS), circ_0001947 knockdown sEVs group treated with 0.9% NS and POM-1 (a CD39 inhibitor), knockdown-control sEVs group treated with anti-PD-1 antibody, and circ_0001947 knockdown sEVs group treated with anti-PD-1 antibody and POM-1. A total of 1×10^6 MFC cells were inoculated into the right side of mice. 60 µg sEVs extracted from sh-NC and sh-circ_001947 MFC cells were injected into the tumor every 3 days starting after the tumor formation, while 10 mg/kg anti-PD-1 antibody and 5 mg/kg POM-1 were intraperitoneally injected every 5 days. Tumor growth was measured every 5 days by monitoring the volumes, which was calculated by the formula: $0.5 \times \text{length} \times \text{width}^2$. The mice were sacrificed after 30 days and tumors were removed for further analysis.

Immunohistochemistry

Paraffin-embedded tumor tissue samples were sectioned into 5 mm. After blocking with 10% bovine serum albumin (BSA) for 1h at room temperature, the samples were incubated with antibodies specific for CD8 (Abcam, ab237709) and migration and invasion markers as Vimentin (Abcam, ab20346) and N-cadherin (Abcam, ab245827) overnight at 4 °C, then incubated with secondary antibodies at room temperature for 1h. The immunohistochemistry images were observed using a microscope.

Bioinformatics analysis

CircRNA sequencing data in GC was obtained from GEO database (GSE131414, GSE152309, and GSE163416). Differentially expressed genes (DEGs) between GC tissues and normal tissues were extracted by using the package "limma" and setting the cutoff as $P < 0.05$. ENCORI database was used to identify miRNAs with binding sites on circ_0001947. Targets can database was used to predict the downstream targets of miRNAs. We obtained single-cell sequencing from TISCH database (GSE183904 and GSE167297) and conducted t-distributed stochastic neighbor embedding (t-SNE) algorithm in the CCA R package to delineate cell clusters. The uniform manifold approximation and projection (UMAP) algorithm was performed to find out CD39 expression across all cell types.

Statistical analysis

The experimental results were analyzed by Student's *t* test (unpaired, two tailed) or one-way ANOVA. The data are presented as the mean \pm standard deviation (SD). $P < 0.05$ was considered as statistically significant. All statistical analyses were performed using GraphPad Prism 8.0 Software.

Results

Circ_0001947 was identified as a novel prognosis-related and overexpressed circRNA in GC cells

We obtained differently expressed GC-associated circRNAs from three datasets in GEO database (Fig. 1A) and found 6 common upregulated circRNAs: circ_0000048, circ_0001821, circ_0001947, circ_0004592, circ_0008433 and circ_0077736 (Fig. 1B). We found that the level of circ_0001947 was higher in GC tissues than that in normal tissues (Fig. 1C) and correlated with poor prognosis for GC patients (Fig. 1D) as well as higher tumor size and TNM stage (Table 1). Further PCR results revealed that circ_0001947 was overexpressed in GC tissues (Fig. 1E). Sanger sequencing verified that backsplice junction site of circ_0001947 (Fig. 1F). Meanwhile, treated by RNase R dampened the level of linear AFF2 mRNA and had no effect on circAFF2 (Fig. 1G). After treating with Actinomycin D, circAFF2 exhibited more stability than linear AFF2 mRNA (Fig. 1H). Furthermore, FISH assay revealed circ_0001947 was localized in the cell cytoplasm (Fig. 1I).

Circ_0001947 was overexpressed in sEVs from GC and promoted GC cell proliferation, migration, and invasion

sEVs were isolated from the plasma of GC patients and detected by electron microscopy and NTA assay, which showed the unique morphology of sEVs with the diameter of 143 nm (Fig. 2A, B). The higher expression of sEVs markers CD63, CD81, and TSG101 and lower expression of calnexin in sEVs from GC further quantified sEVs (Fig. 2C). circ_0001947 has the highest levels among the 6 upregulated circRNAs mentioned above in GC-derived sEVs, while no significant difference was found among circ_0001947, circ_0004592, and circ_0077736 (Fig. 2D). Then, we established stable knockdown of circ_0001947, circ_0004592, and circ_0077736 to explore their effect on GC. CCK-8 assay showed a significant decrease in proliferative ability after inhibiting circ_0001947 expression (Fig. 2E), but no significant difference was found after inhibiting circ_0004592 or circ_0077736 expression (Figure S1A, B). Transwell and wound healing assay confirmed the invasion and migration of GC cells was restricted by circ_0001947 knockdown (Fig. 2F, G), while circ_0004592 or circ_0077736 knockdown exerted no significant effect on the invasion and migration of GC cells revealed by transwell (Figure S1C, D) and wound healing assay (Figure S1E, F). MFC cells transfected with

sh-NC or sh-circ_0001947 were inoculated into the mice and we found a obviously dampened tumor growth sh-circ_0001947, indicating that circ_0001947 stimulated tumor progression in vivo (Fig. 2H, I).

Circ_0001947 served as a sponge of miR-661 and miR-671-5p

Former research has proved that circRNAs could perform functions as competitive endogenous RNAs to mediate miRNA expression [27]. To explore the underlying mechanism of circ_0001947, we used ENCORI database to find out downstream miRNAs interacting with circ_0001947. As revealed by ENCORI database, circ_0001947 could bind to miR-661 and miR-671-5p (Fig. 3A). We conducted RIP assay in GC cells and the results indicated that endogenous circ_0001947 was enriched (Fig. 3B), suggesting the possibility of circ_0001947 functioning as miRNA sponge. Dual-luciferase assay verified that miR-661 and miR-671-5p mimics decreased the luciferase activity of WT circ_0001947 rather than MT circ_0001947 (Fig. 3C, D). The levels of miR-661 and miR-671-5p were significantly upregulated after decreasing circ_0001947 expression (Fig. 3E). The expression of miR-661 and miR-671-5p was found obviously decreased in GC tissues than normal tissues (Fig. 3F). To analyze whether circ_0001947 promoted GC progression by binding to miR-661 or miR-671-5p, we performed a miR-661 or miR-671-5p mimics co-transfected with sh-circ_0001947 into GC cells. CCK-8 (Fig. 3G), transwell (Fig. 3H) and wound healing assay (Fig. 3I) demonstrated that circ_0001947 knockdown could reduce the proliferation, migration, and invasion phenotype of GC cells, while miR-661 or miR-671-5p inhibitors partly abolished the function of circ_0001947 knockdown. Taken together, circ_0001947 stimulated GC progression by acting as miR-661 or miR-671-5p sponge.

CD39 was targeted by miR-661 or miR-671-5p

To analyze the downstream of miR-661 and miR-671-5p, we utilized TargetScan database to find out the target gene CD39 (ENTPD1) (Fig. 4A, B). Meanwhile, CD39 was demonstrated to positively correlate to circ_0001947 expression (Fig. 4C). Previous studies have demonstrated that CD39 expressed on CD8⁺ T cells participated in regulating T cells exhaustion [24]. Then, we conducted single-cell sequencing analysis of CD39 expression in two GC single-cell datasets (GSE183904, GSE167297), and we found that CD39 expression exhibited a positive relationship with the presence of CD8⁺ T cells (Fig. 4D, E). For sEVs tracking, GC-derived sEVs were labeled with PKH-26, and the result revealed that sEVs were effectively absorbed by CD8⁺ T cells (Fig. 4F). Subsequently, we treated CD8⁺ T cells with sEVs from GC cells and

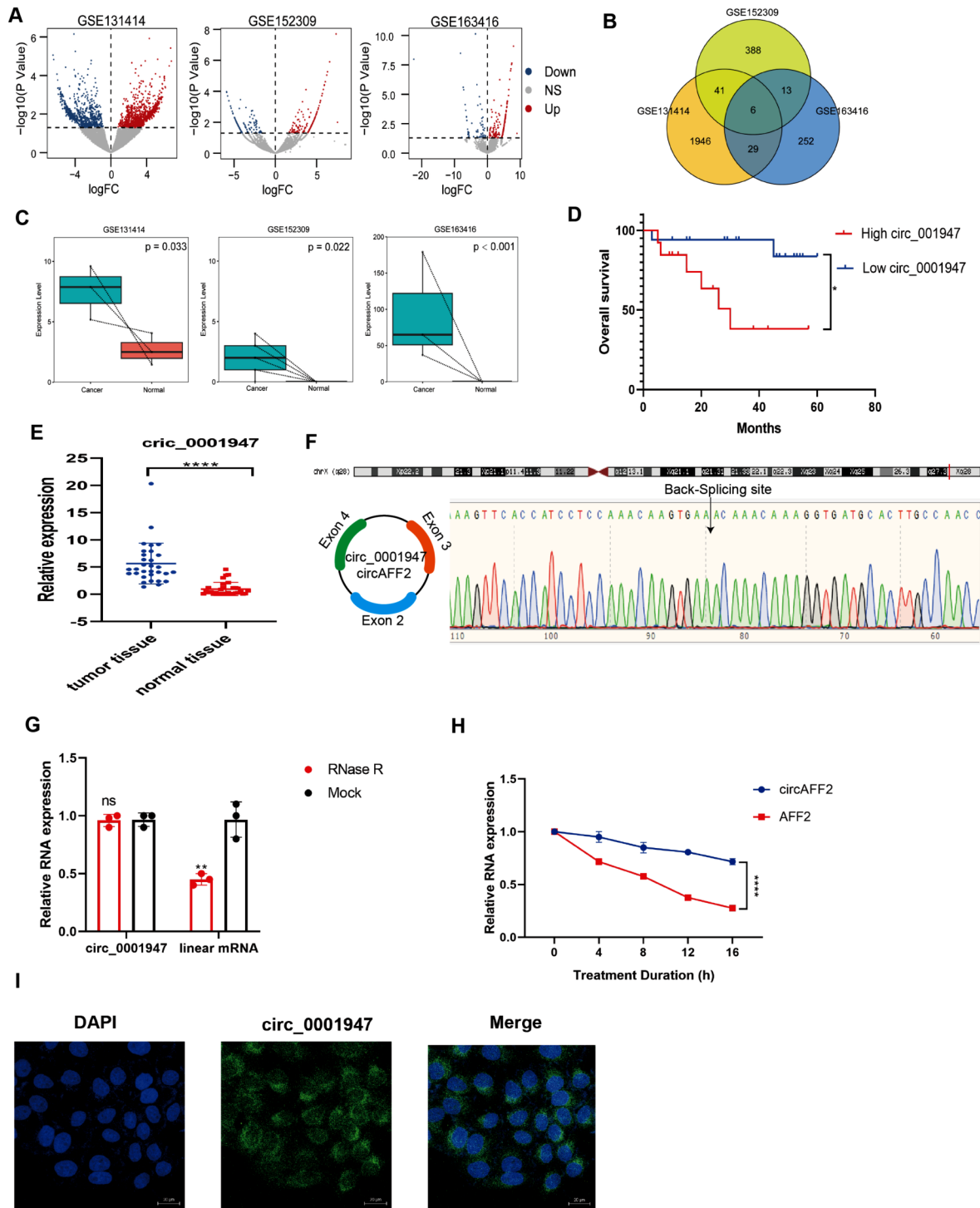


Fig. 1 Circ_0001947 was identified as a novel prognosis-related and overexpressed circRNA in GC cells. **A** Volcano plots based on the DEGs between GC and normal tissues analyzed from GEO datasets GSE131414, GSE152309, and GSE163416. **B** Common DEGs from three datasets. **C** Circ_0001947 was upregulated in GC. **D** Circ_0001947 expression was negatively correlated with overall survival. **E** Circ_0001947 was upregulated in GC tissues detected by PCR assay. **F** The genomic loci and circular structure of circ_0001947, which was verified by Sanger sequencing. **G** Expression of circular and linear AFF2 in AGS cells after RNase R treatment. **H** Expression of circular and linear AFF2 in AGS cells treated with Actinomycin D. **I** Circ_0001947 was located in cell cytoplasm revealed by -FISH assay. Scale bar, 20 μm . * $P < 0.05$; ** $P < 0.01$; *** $P < 0.001$; **** $P < 0.0001$. NS, not significant

Table 1 Correlation of circ_0001947 expression and clinicopathological features in GC

Parameters	Number of patients	circ_0001947 expression		P value
		Low	High	
Gender				
Male	18	8	10	0.999
Female	12	5	7	
Age(years)				
≥60	19	7	12	0.454
<60	11	6	5	
Tumor location				
Upper	21	7	14	0.123
Lower	9	6	3	
Tumor diameter				
≥5 cm	20	5	15	0.007
<5 cm	10	8	2	
Tumor infiltration depth				
Intraserous	13	4	9	0.283
Extraserous	17	9	8	
TNM stage				
I-II	8	6	2	0.049
III-IV	22	7	15	
Differentiation				
Well	9	2	7	0.229
Poor	21	11	10	
Lymph node metastasis				
Yes	17	10	7	0.071
No	13	3	10	
Vessel invasion				
Yes	11	6	5	0.454
No	19	7	12	
Distant metastasis				
Yes	4	1	3	0.613
No	26	12	14	

supplemented with miR-661 or miR-671-5p mimics and inhibitors. The WB results verified that CD39 expression in CD8⁺ T cells was obviously downregulated after treatment of miR-661 or miR-671-5p mimics, while miR-661 or miR-671-5p inhibitors further promoted sEVs-induced CD39 expression (Fig. 4G, H). In conclusion, these results confirmed that CD39 was targeted by miR-661 and miR-671-5p.

sEVs carried circ_0001947 induced CD8⁺ T cell exhaustion

CD39 was identified to serve as a crucial regulatory role in CD8⁺ T cell exhaustion. In consideration of sEVs-encapsulated circ_0001947 was abundant in GC tissues and it could target CD39, we further explored its effect on CD8⁺ T cell exhaustion. According to the circ_0001947 expression in GC tissues detected by PCR assay, we divided our 30-patient tissues into two groups. Interestingly, we found that circ_0001947-high group had lower CD8⁺ T cell infiltration, which was confirmed by

immunohistochemical results (Fig. 5A, S2). CD8⁺ T cells were isolated from PBMCs of healthy donors and identified as CD45⁺/CD3⁺/CD8⁺ cells (Figure S3). Then we co-cultured CD8⁺ T cells with AGS cells for further study, and sEVs from sh-NC or sh-circ_001947 were added to the treatment (Fig. 5B). At the same time, POM-1 was added to inhibit CD39 expression. We found that the level of IFN- γ (Fig. 5C), perforin (Fig. 5D), and GZMB (Fig. 5E) on CD8⁺ T cells was elevated through inhibiting sEVs carried circ_0001947 and CD39. Conversely, the level of PD-1 (Fig. 5F) and Tim-3 (Fig. 5G) was reduced by inhibiting sEVs carried circ_0001947 and CD39. These results indicated that circ_0001947 encapsulated by sEVs induced CD8⁺ T cell exhaustion.

sEVs carried circ_0001947 contributed to immune resistance in GC

It has been reported that CD8⁺ T cell exhaustion was an important factor in immune resistance modulation, so we explored whether sEVs-packaged circ_0001947 could modulate immune resistance through mediating CD8⁺ T cell exhaustion. To evaluate the function of sEVs carried circ_0001947 on anti-PD-1 efficacy, sEVs from sh-NC or sh-circ_0001947 were injected into mice. Meanwhile, the mice were treated with 0.9% NS, POM-1 or anti-PD-1 antibody. We found that sh-circ_0001947 carried by sEVs combined with CD39 inhibitor significantly reduced tumor growth rate (Fig. 6A, B) and tumor weight (Fig. 6C). Moreover, flow cytometry results showed that infiltrated CD8⁺ T cells were increased after CD39 knockdown and anti-PD-1 treatment (Fig. 6D). Immunohistochemistry analysis revealed that the expressions of migration and invasion markers as Vimentin and N-cadherin were attenuated after sEVs carried sh-circ_0001947 treatment and that they further suppressed by CD39 knockdown and anti-PD-1 treatment (Fig. 6E). Taken together, our results demonstrated that circ_0001947 encapsulated by sEVs facilitated anti-PD-1 resistance in GC (Fig. 6F).

Discussion

A well-known hallmarks of cancer is to escape from immune surveillance and contribute to immune resistance 28. In the past decades, a variety of cancer research focused on discover new checkpoints such as SMAR-CAL1, CD3LI, and IGSF8 29–31. However, the solution to overcome immune resistance and improve existing checkpoints efficacy remains largely overlooked. With the development of novel technologies like single-cell sequencing and high-throughput sequencing, thousands of circRNAs were identified and their functions endowed by stable structures in cancers were further explored 32, 33. In this study, we screened differential circRNA profiles of GC tissues from RNA-seq data from GEO

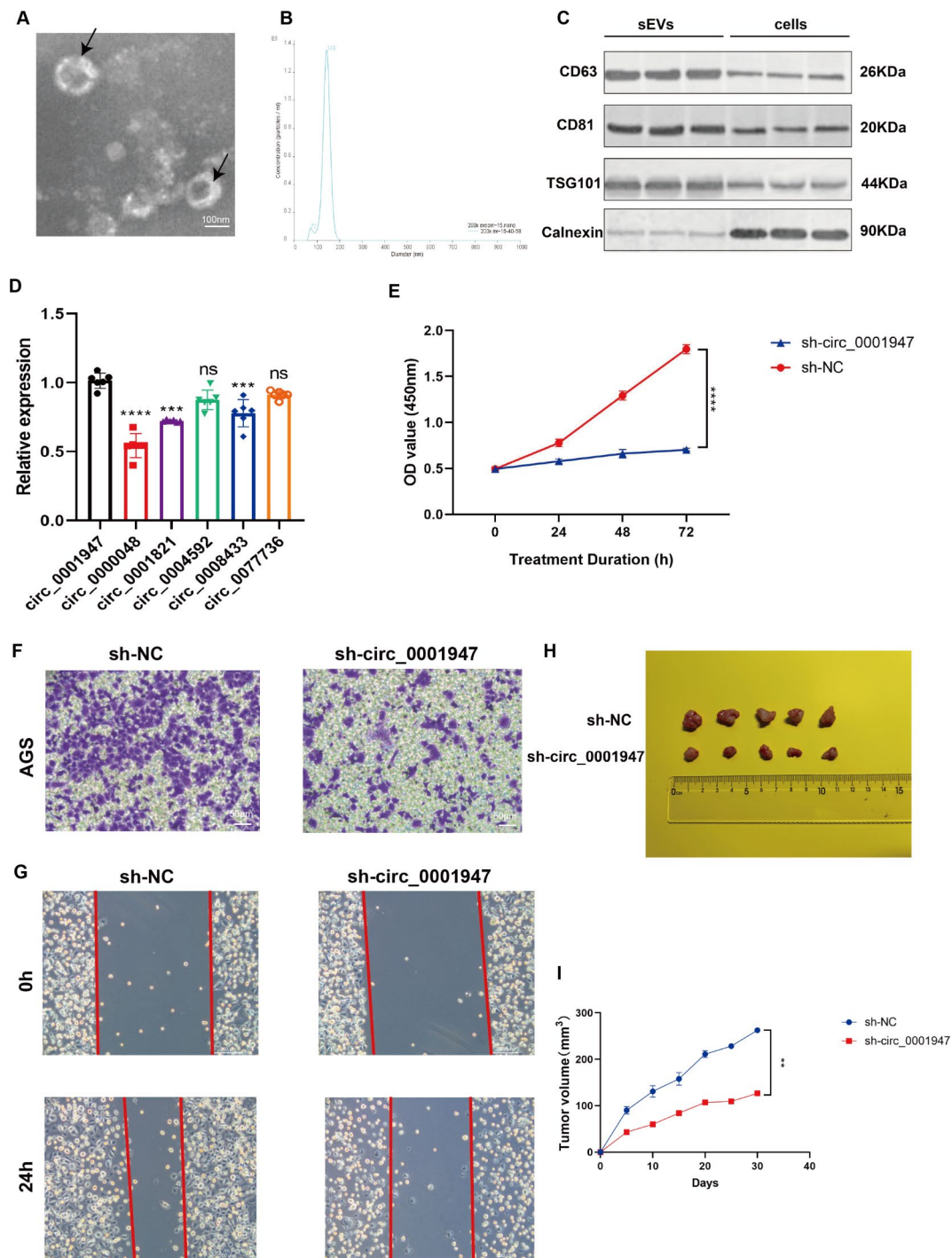


Fig. 2 Circ_0001947 was overexpressed in sEVs from GC and promoted GC cell proliferation, migration, and invasion. **A** Transmission electron microscope images of sEVs from GC. Scale bar, 100 nm. **B** NTA analysis of sEVs from GC. **C** WBA assay of positive and negative biomarkers in AGS-derived sEVs and cells. **D** Expression of 6 circRNAs in GC-derived sEVs. **E** CCK-8 assay of AGS cells transfected with sh-NC and sh-circ_0001947. **F** Transwell assay of AGS cells transfected with sh-NC and sh-circ_0001947. Scale bar, 50 μm. **G** Wound healing assay of AGS cells transfected with sh-NC and sh-circ_0001947. Scale bar, 200 μm. **H** General images of subcutaneous xenograft tumor model. **I** Tumor growth curved of subcutaneous xenograft tumor model. * $P < 0.05$; ** $P < 0.01$; *** $P < 0.001$; **** $P < 0.0001$; NS, not significant

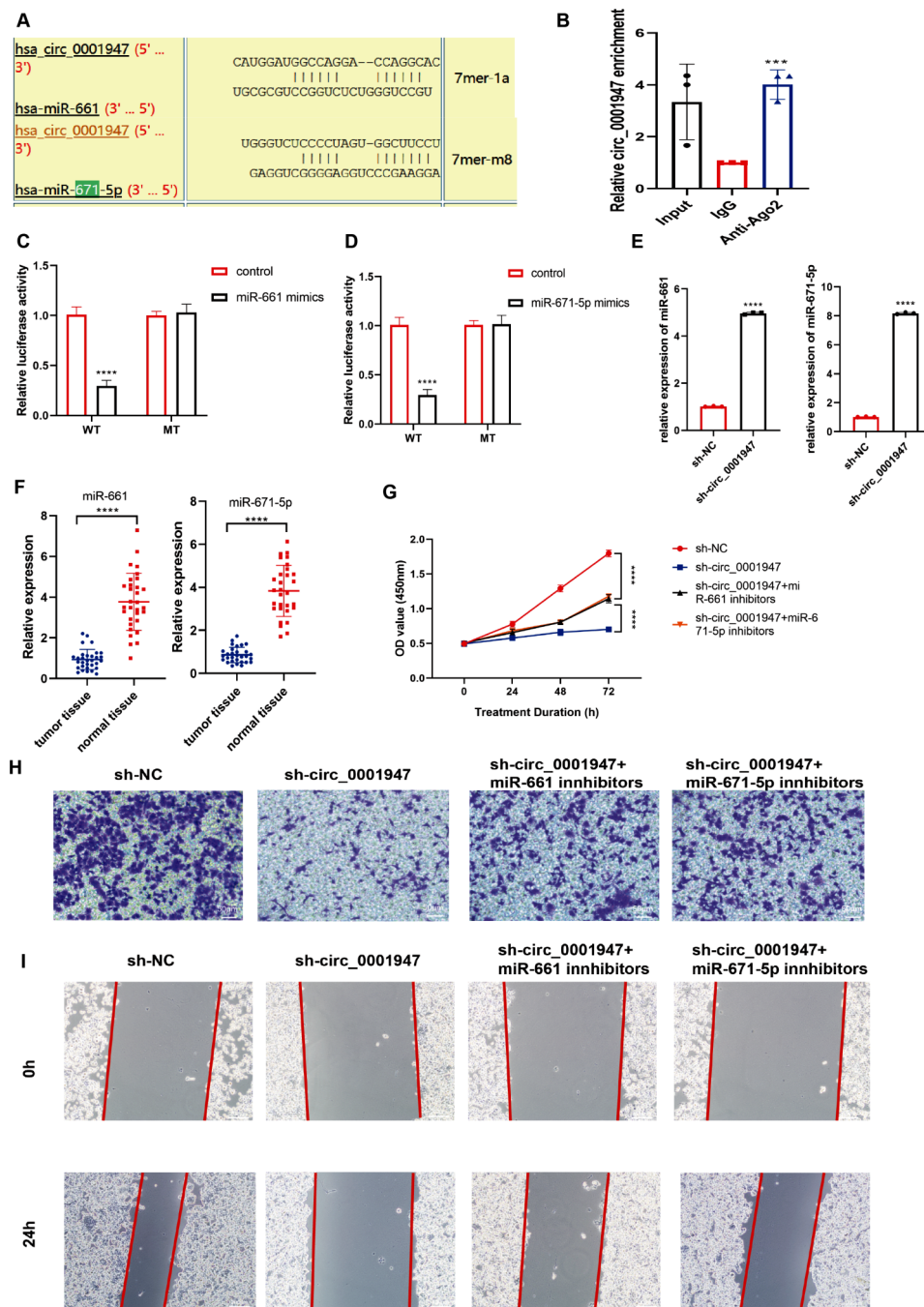


Fig. 3 Circ_0001947 served as a sponge of miR-661 and miR-671-5p. **A** The predicted binding sites between circ_0001947 and miR-661, miR-671-5p revealed by ENCORI database. **B** RIP results of circ_0001947 in Ago2 immunoprecipitations. **C** Dual-luciferase assay showed the binding properties of circ_0001947 and miR-661. **D** Dual-luciferase assay showed the binding properties of circ_0001947 and miR-671-5p. **E** PCR assay of miR-661 and miR-671-5p expression after circ_0001947 knockdown. **F** MiR-661 and miR-671-5p expression was downregulated in GC tissues detected by PCR assay. **G** CCK-8 assay of AGS cells transfected with sh-NC, sh-circ_0001947, sh-circ_0001947 + miR-661 inhibitors and sh-circ_0001947 + miR-671-5p inhibitors. **H** Transwell assay of AGS cells transfected with sh-NC, sh-circ_0001947, sh-circ_0001947 + miR-661 inhibitors and sh-circ_0001947 + miR-671-5p inhibitors. Scale bar, 50 μ m. **I** Wound healing assay of AGS cells transfected with sh-NC, sh-circ_0001947, sh-circ_0001947 + miR-661 inhibitors and sh-circ_0001947 + miR-671-5p inhibitors. Scale bar, 200 μ m. *** P < 0.001; **** P < 0.0001

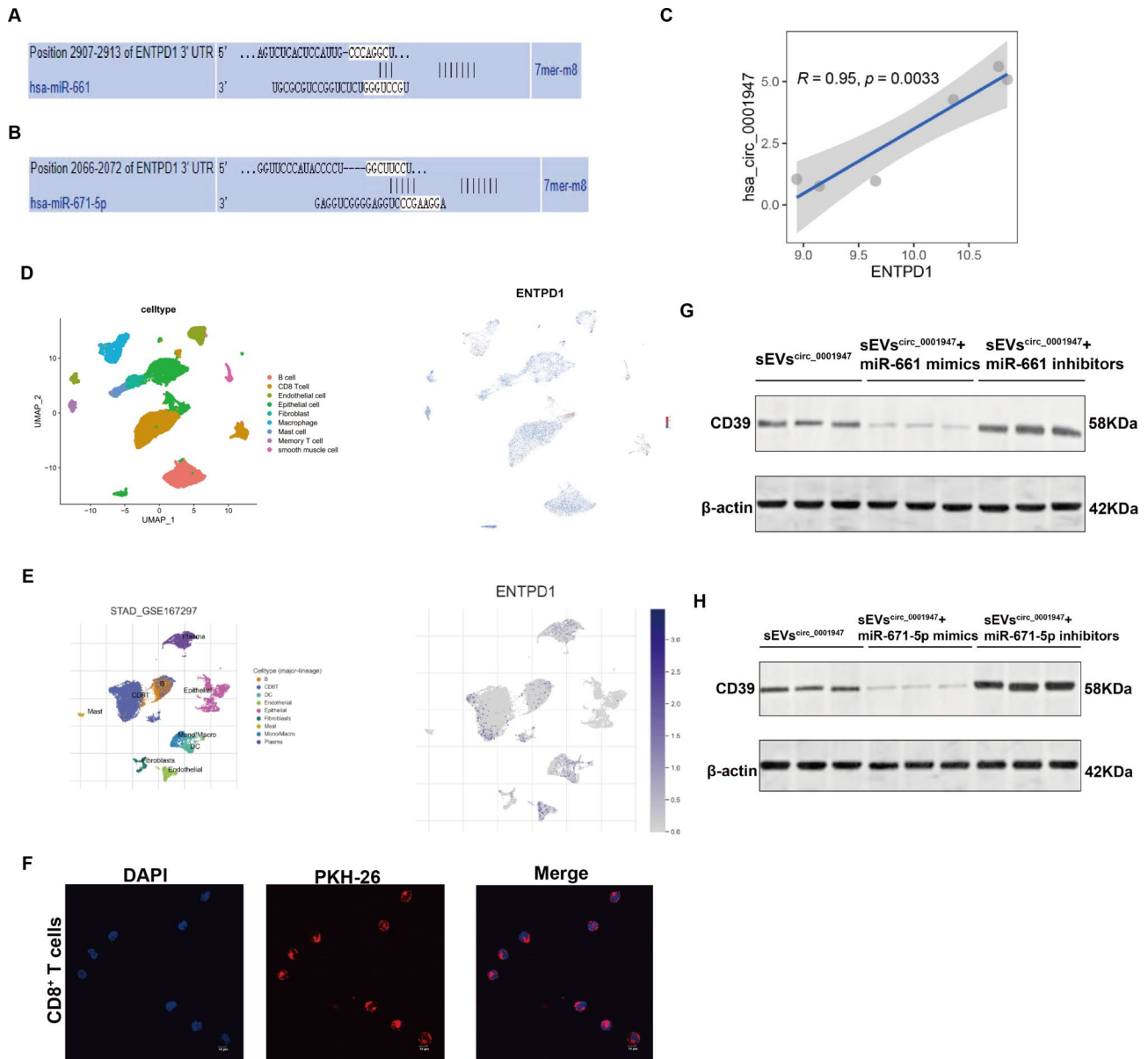


Fig. 4 CD39 was targeted by miR-661 or miR-671-5p. **A** The predicted binding sites between miR-661 and CD39 revealed by TargetScan database. **B** The predicted binding sites between miR-671-5p and CD39 revealed by TargetScan database. **C** Correlation between expression of circ_0001947 and CD39 in GC. **D-E** Validation of CD39 (ENTPD1) expression in two gastric single-cell datasets (GSE183904, GSE167297). From left to right, cell cluster plot and CD39 expression plot in different cells. **F** Representative images of the internalization of PKH-26-labeled sEVs (red) by CD8⁺ T cells. Scale bar, 10 μ m. **G** WB assay of CD39 expression in CD8⁺ T cell transfected with sEVs^{circ_0001947}, sEVs^{circ_0001947} and miR-661 mimics, or sEVs^{circ_0001947} and miR-661 inhibitors. **H** WB assay of CD39 expression in CD8⁺ T cell transfected with sEVs^{circ_0001947}, sEVs^{circ_0001947} and miR-671-5p mimics, or sEVs^{circ_0001947} and miR-671-5p inhibitors

datasets and identified circ_0001947, related to worse prognosis, was overexpressed in GC tissues.

Emerging research has reported that circRNAs often exerted their effects as an oncogenic regulator in GC. CircCUL2 contributed to malignant transformation of GC by sponging miR-142-3p to mediate ROCK2 expression [34]. Circ50547 promoted gastric carcinogenesis through acting as a miR-217 sponge and modulating HNF1B expression [35]. CircSTRBP was found to perform

its function via miR-1294/miR-593-3p/E2F2 axis, thereby inducing GC progression [36]. CiRS-7 was verified to inhibit the miR-7-regulated PTEN/PI3K/AKT pathway, which ultimately facilitated GC progression [37]. Thus, we investigated the role of circ_0001947 in GC. We found that overexpressed circ_0001947 obviously led to the proliferation, migration, and invasion of GC cells. Reciprocally, downregulated circ_0001947 significantly

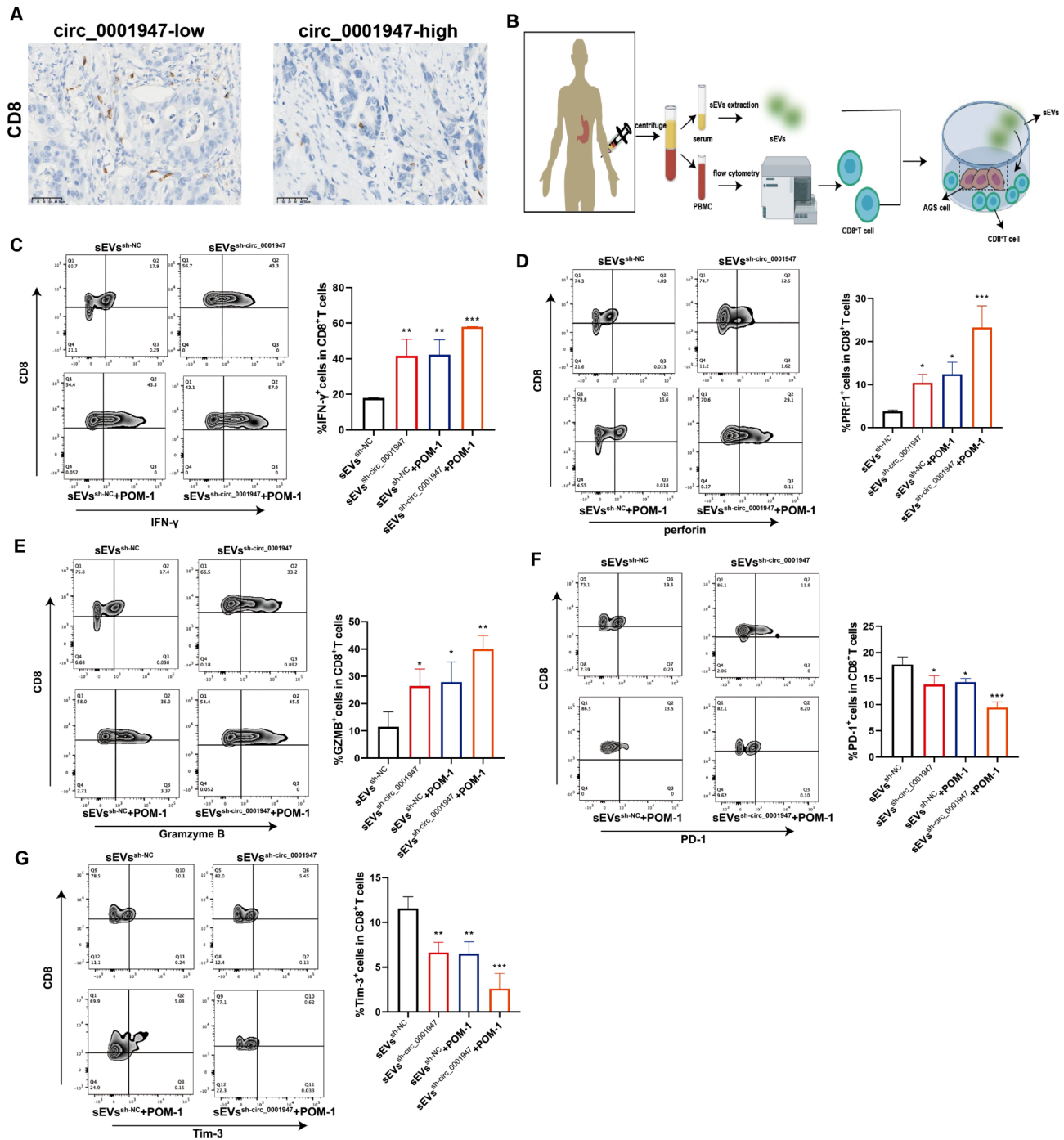


Fig. 5 sEVs carried circ_0001947 induced CD8⁺ T cell exhaustion. **A** Representative images of immunohistochemical staining on CD8 in 30 GC patients. Scale bar, 50 μ m. **B** Co-culture of CD8⁺ T cells treated with sEVs and AGS cells. **C–E** Percentage of IFN- γ ⁺ (**C**), perforin⁺ (**D**), and GZMB⁺ (**E**) in CD8⁺ T cells after treating with sEVs^{circ_0001947} and/or POM-1 detected by flow cytometry. **F–G** Percentage of PD-1⁺ (**F**) and Tim-3⁺ (**G**) in CD8⁺ T cells after treating with sEVs^{circ_0001947} and/or POM-1 detected by flow cytometry. * $P < 0.05$; ** $P < 0.01$; *** $P < 0.001$

suppressed the proliferation, migration, and invasion of GC cells in vivo and vitro.

When exploring the mechanism underlying the regulatory effect of circ_0001947 on GC progression, we conducted bioinformatic analysis to find out miR-661 and miR-671-5p as the downstream targets of circ_0001947.

Additionally, we found the upregulated expression of miR-661 and miR-671-5p after circ_0001947 knock-down. Increasing evidence indicated that circRNAs could perform their functions by sponging miRNAs to regulate protein-coding genes [38, 39]. In our study, the RIP assay confirmed the enrichment of circ_0001947 in AGO2

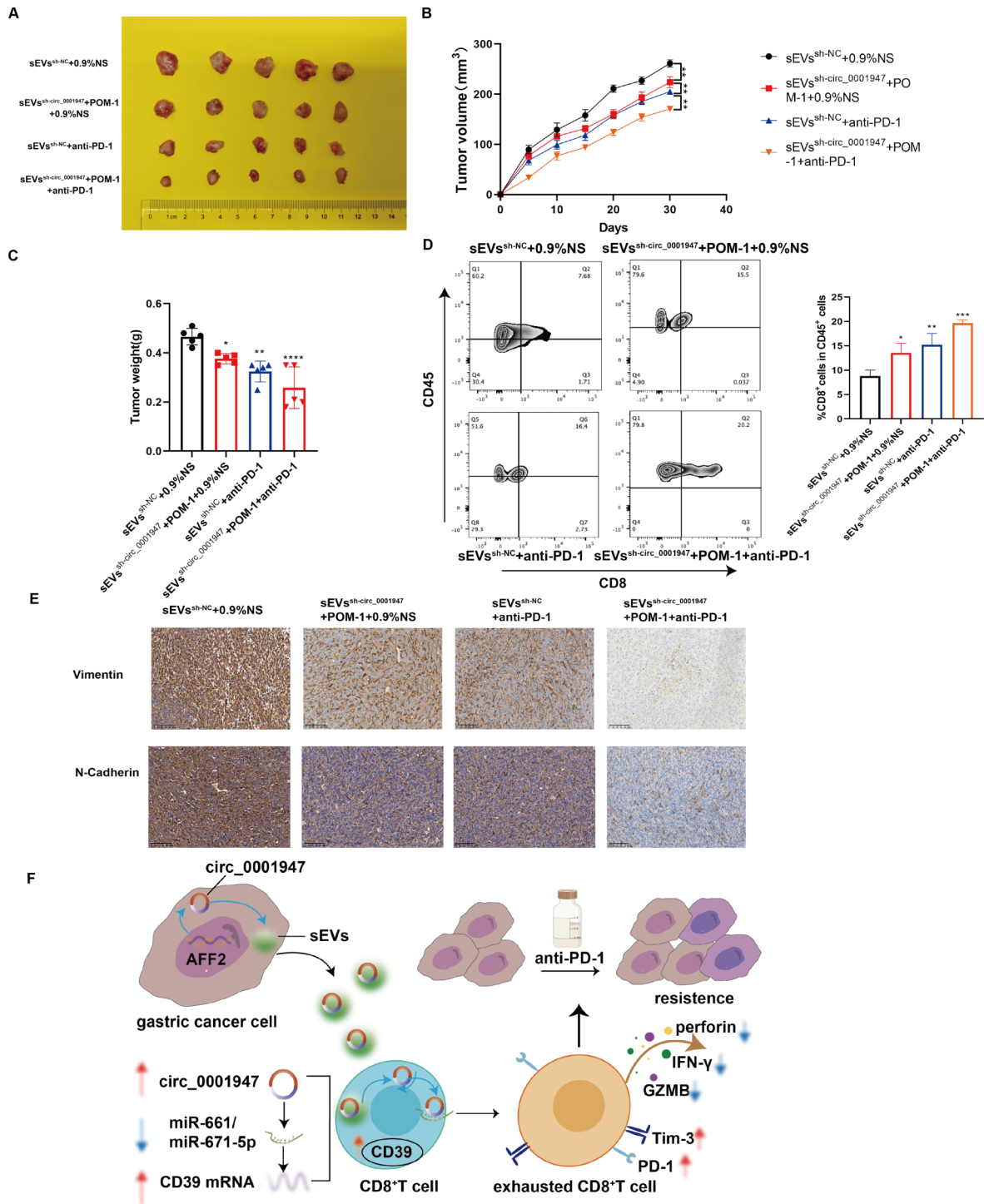


Fig. 6 sEVs carried circ_0001947 contributed to immune resistance in GC. **A** General images of subcutaneous xenograft tumor model. **B** Tumor growth curve of subcutaneous xenograft tumor model. **C** Tumor weight curve of subcutaneous xenograft tumor model. **D** Comparison of expression of CD8⁺/CD45⁺ cells in tumors detected by flow cytometry. **E** Immunohistochemical staining of Vimentin and N-cadherin after treating with sEVs^{sh-circ_0001947} and/or POM-1 and/or anti-PD-1. Scale bar, 100 μm. **F** Schematic diagram of sEVs-packaged circ_0001947 in GC tumor microenvironment. **P* < 0.05; ***P* < 0.01; ****P* < 0.001; *****P* < 0.0001

immunoprecipitation and dual-luciferase assay identified the direct relationship of miR-661, miR-671-5p and circ_0001947. Meanwhile, the enhanced of miR-661 and miR-671-5p could significantly dampen the proliferation, invasion, and migration of GC induced by circ_0001947.

sEVs could carry proteins, DNAs, and RNAs that remodel the complicated TME, which may ultimately alter the response to ICB 40, 41. For example, miR-142-3p contained by sEVs promoted apoptosis in T cells to affect immunosuppression 42. Head and neck squamous cell carcinoma (HNSCC) derived sEVs containing CD73 activated NF- κ B pathway in macrophages, thereby contributing to immunosuppression 43. In this study, we reported that circ_0001947 was stable present in GC derived sEVs with remarkably upregulated expression. Circ_0001947 encapsulated by sEVs from GC cells was able to increase the expression of Tim-3 and PD-1 while decrease the expression of IFN- γ , GZMB, and perforin in T cells, implying that sEVs-carried circ_0001947 facilitated CD8⁺ T cell exhaustion. In addition, CD8⁺ T cell exhaustion caused by sEVs-carried circ_0001947 led to the resistance to anti-PD-1 therapy in GC. Furthermore, we explored the mechanism by which sEVs-carried circ_0001947 contributed to CD8⁺ T cell exhaustion. In our research, we found that CD39 expressed on CD8⁺ T cell was the downstream target of miR-661 and miR-671-5p. Previous studies have demonstrated CD39 was a vital regulator in T cell function 44, 45. CD8⁺ T cell exhaustion and immune resistance were rescued after inhibiting CD39 expression induced by sEVs-carried circ_0001947, indicating that circ_0001947 encapsulated by sEVs contributed to CD8⁺ T cell exhaustion and immune escape through sponging miR-661 and miR-671-5p to elevate CD39 level in GC.

In summary, our study demonstrated the oncogenic role of circ_0001947 as promoting proliferation, invasion, and migration of GC. sEVs-carried circ_0001947 could act as miR-661 or miR-671-5p sponge to upregulate CD39, a key regulator in T cell function. The overexpressed CD39 contributed to CD8⁺ T cell exhaustion and resistance of GC cells to anti-PD-1 therapy, which caused the immunosuppressive TME. Thus, our study open up new avenues for overcoming immune escape in GC.

Supplementary Information

The online version contains supplementary material available at <https://doi.org/10.1186/s12951-024-02826-5>.

Supplementary Material 1

Author contributions

Bibo Tan and Mingming Zhang designed and supervised the study; Bingyu Wang, Wenbo Liu and Hongyue Tang performed the experiments; Yong Li provided administrative, technical, and material support; Yingying Wang, Chao

Song, and Buyun Song analyzed the data; Bingyu Wang wrote and revised the manuscript. All authors read and approved the final manuscript.

Funding

This work was supported by the Health Commission of Hebei Province [20230123]; Hebei Medical University [2022LCTD-A13]; Hebei Provincial Department of Science and Technology [22377701D].

Data availability

No datasets were generated or analysed during the current study.

Declarations

Ethical approval

All tissues and bloods was obtained from patients with informed consent, and all related procedures were approved with the approval of the internal review and ethics boards of the Fourth Affiliated Hospital of Hebei Medical University. All mice were kept by experienced animal keepers in sterile animal rooms following the ARRIVE guidelines and approved by the Committee on the Ethics of Animal Experiments of Hebei Medical University.

Competing interests

The authors declare no competing interests.

Received: 27 May 2024 / Accepted: 31 August 2024

Published online: 14 September 2024

References

1. Bray F, Ferlay J, Soerjomataram I, Siegel RL, Torre LA, Jemal A. Global cancer statistics 2018: GLOBOCAN estimates of incidence and mortality worldwide for 36 cancers in 185 countries. *CA Cancer J Clin.* 2018;68(6):394–424.
2. Poggio M, Hu T, Pai CC, Chu B, Belair CD, Chang A, et al. Suppression of exosomal PD-L1 induces systemic anti-tumor immunity and memory. *Cell.* 2019;177(2):414–27. e13.
3. Janjigian YY, Kawazoe A, Yanez P, Li N, Lonardi S, Kolesnik O, et al. The KEYNOTE-811 trial of dual PD-1 and HER2 blockade in HER2-positive gastric cancer. *Nature.* 2021;600(7890):727–30.
4. Hogner A, Moehler M. Immunotherapy in Gastric Cancer. *Curr Oncol.* 2022;29(3):1559–74.
5. Shitara K, Van Cutsem E, Bang YJ, Fuchs C, Wyrwicz L, Lee KW, et al. Efficacy and safety of Pembrolizumab or Pembrolizumab Plus Chemotherapy vs Chemotherapy alone for patients with First-line, Advanced Gastric Cancer: the KEYNOTE-062 phase 3 Randomized Clinical Trial. *JAMA Oncol.* 2020;6(10):1571–80.
6. Muro K, Chung HC, Shankaran V, Geva R, Catenacci D, Gupta S, et al. Pembrolizumab for patients with PD-L1-positive advanced gastric cancer (KEYNOTE-012): a multicentre, open-label, phase 1b trial. *Lancet Oncol.* 2016;17(6):717–26.
7. Wang Z, Wang Y, Gao P, Ding J. Immune checkpoint inhibitor resistance in hepatocellular carcinoma. *Cancer Lett.* 2023;555:216038.
8. Fei X, Li Z, Yang D, Kong X, Lu X, Shen Y, et al. Neddylation of Coro1a determines the fate of multivesicular bodies and biogenesis of extracellular vesicles. *J Extracell Vesicles.* 2021;10(12):e12153.
9. Thery C, Witwer KW, Aikawa E, Alcaraz MJ, Anderson JD, Andriantsitohaina R, et al. Minimal information for studies of extracellular vesicles 2018 (MISEV2018): a position statement of the International Society for Extracellular Vesicles and update of the MISEV2014 guidelines. *J Extracell Vesicles.* 2018;7(1):1535750.
10. Brown MC, Mosaheb MM, Mohme M, McKay ZP, Holl EK, Kastan JP, et al. Viral infection of cells within the tumor microenvironment mediates antitumor immunotherapy via selective TBK1-IRF3 signaling. *Nat Commun.* 2021;12(1):1858.
11. Qu Z, Jiang C, Wu J, Ding Y. Exosomes as potent regulators of HCC malignancy and potential bio-tools in clinical application. *Int J Clin Exp Med.* 2015;8(10):17088–95.
12. Han QF, Li WJ, Hu KS, Gao J, Zhai WL, Yang JH, et al. Exosome biogenesis: machinery, regulation, and therapeutic implications in cancer. *Mol Cancer.* 2022;21(1):207.

13. Qu S, Yang X, Li X, Wang J, Gao Y, Shang R, et al. Circular RNA: a new star of noncoding RNAs. *Cancer Lett.* 2015;365(2):141–8.
14. Chen DL, Sheng H, Zhang DS, Jin Y, Zhao BT, Chen N, et al. The circular RNA circDLG1 promotes gastric cancer progression and anti-PD-1 resistance through the regulation of CXCL12 by sponging miR-141-3p. *Mol Cancer.* 2021;20(1):166.
15. Yao W, Guo P, Mu Q, Wang Y. Exosome-derived Circ-PVT1 contributes to Cisplatin Resistance by regulating Autophagy, Invasion, and apoptosis Via miR-30a-5p/YAP1 Axis in Gastric Cancer cells. *Cancer Biother Radiopharm.* 2021;36(4):347–59.
16. Zhang C, Wei G, Zhu X, Chen X, Ma X, Hu P, et al. Exosome-delivered circ-STAU2 inhibits the progression of gastric Cancer by targeting the miR-589/CAPZA1 Axis. *Int J Nanomed.* 2023;18:127–42.
17. Zhang PF, Gao C, Huang XY, Lu JC, Guo XJ, Shi GM, et al. Cancer cell-derived exosomal circUHRF1 induces natural killer cell exhaustion and may cause resistance to anti-PD1 therapy in hepatocellular carcinoma. *Mol Cancer.* 2020;19(1):110.
18. Shibutani M, Maeda K, Nagahara H, Fukuoka T, Nakao S, Matsutani S, et al. The Prognostic significance of the Tumor-infiltrating programmed cell Death-1(+) to CD8(+) lymphocyte ratio in patients with colorectal Cancer. *Anticancer Res.* 2017;37(8):4165–72.
19. Mittrucker HW, Visekruna A, Huber M. Heterogeneity in the differentiation and function of CD8(+) T cells. *Arch Immunol Ther Exp (Warsz).* 2014;62(6):449–58.
20. Okadome K, Baba Y, Yagi T, Kiyozumi Y, Ishimoto T, Iwatsuki M, et al. Prognostic Nutritional Index, Tumor-infiltrating lymphocytes, and prognosis in patients with esophageal Cancer. *Ann Surg.* 2020;271(4):693–700.
21. Wherry EJ, Kurachi M. Molecular and cellular insights into T cell exhaustion. *Nat Rev Immunol.* 2015;15(8):486–99.
22. Wang Q, Qin Y, Li B. CD8(+) T cell exhaustion and cancer immunotherapy. *Cancer Lett.* 2023;559:216043.
23. Canale FP, Ramello MC, Nunez N, Araujo Furlan CL, Bossio SN, Gorosito Serran M, et al. CD39 expression defines cell exhaustion in Tumor-infiltrating CD8(+) T cells. *Cancer Res.* 2018;78(1):115–28.
24. Zhang Y, Hu J, Ji K, Jiang S, Dong Y, Sun L, et al. CD39 inhibition and VISTA blockade may overcome radiotherapy resistance by targeting exhausted CD8+T cells and immunosuppressive myeloid cells. *Cell Rep Med.* 2023;4(8):101151.
25. Zhao W, Cui Y, Liu L, Qi X, Liu J, Ma S, et al. Splicing factor derived circular RNA circUHRF1 accelerates oral squamous cell carcinoma tumorigenesis via feedback loop. *Cell Death Differ.* 2020;27(3):919–33.
26. Cui Y, Wu Y, Wang C, Wang Z, Li Y, Jiang Z, et al. Isoliquiritigenin inhibits non-small cell lung cancer progression via m(6)A/IGF2BP3-dependent TWIST1 mRNA stabilization. *Phytomedicine.* 2022;104:154299.
27. Li R, Jiang J, Shi H, Qian H, Zhang X, Xu W. CircRNA: a rising star in gastric cancer. *Cell Mol Life Sci.* 2020;77(9):1661–80.
28. Hanahan D. Hallmarks of Cancer: New dimensions. *Cancer Discov.* 2022;12(1):31–46.
29. Leuzzi G, Vasciaveo A, Tagliatalata A, Chen X, Firestone TM, Hickman AR, et al. SMARCAL1 is a dual regulator of innate immune signaling and PD-L1 expression that promotes tumor immune evasion. *Cell.* 2024;187(4):861–81. e32.
30. Deng S, Zhang Y, Wang H, Liang W, Xie L, Li N, et al. ITPRIPL1 binds CD3epsilon to impede T cell activation and enable tumor immune evasion. *Cell.* 2024;187(9):2305–e2333.
31. Li Y, Wu X, Sheng C, Liu H, Liu H, Tang Y et al. IGSF8 is an innate immune checkpoint and cancer immunotherapy target. *Cell.* 2024.
32. Xu X, Zhang J, Tian Y, Gao Y, Dong X, Chen W, et al. CircRNA inhibits DNA damage repair by interacting with host gene. *Mol Cancer.* 2020;19(1):128.
33. Li B, Zhu L, Lu C, Wang C, Wang H, Jin H, et al. circNDUFB2 inhibits non-small cell lung cancer progression via destabilizing IGF2BPs and activating anti-tumor immunity. *Nat Commun.* 2021;12(1):295.
34. Peng L, Sang H, Wei S, Li Y, Jin D, Zhu X, et al. circCUL2 regulates gastric cancer malignant transformation and cisplatin resistance by modulating autophagy activation via miR-142-3p/ROCK2. *Mol Cancer.* 2020;19(1):156.
35. Zang X, Wang R, Wang Z, Qiu S, Zhang F, Zhou L, et al. Exosomal circ50547 as a potential marker and promoter of gastric cancer progression via miR-217/HNF1B axis. *Transl Oncol.* 2024;45:101969.
36. Wang Y, Zou R, Li D, Gao X, Lu X. Exosomal circSTRBP from cancer cells facilitates gastric cancer progression via regulating miR-1294/miR-593-3p/E2F2 axis. *J Cell Mol Med.* 2024;28(8):e18217.
37. Pan H, Li T, Jiang Y, Pan C, Ding Y, Huang Z, et al. Overexpression of circular RNA circS-7 abrogates the Tumor Suppressive Effect of miR-7 on gastric Cancer via PTEN/PI3K/AKT signaling pathway. *J Cell Biochem.* 2018;119(1):440–6.
38. Luo Z, Rong Z, Zhang J, Zhu Z, Yu Z, Li T, et al. Circular RNA circCCDC9 acts as a miR-6792-3p sponge to suppress the progression of gastric cancer through regulating CAV1 expression. *Mol Cancer.* 2020;19(1):86.
39. Bak RO, Mikkelsen JG. miRNA sponges: soaking up miRNAs for regulation of gene expression. *Wiley Interdiscip Rev RNA.* 2014;5(3):317–33.
40. Li C, Ni YQ, Xu H, Xiang QY, Zhao Y, Zhan JK, et al. Roles and mechanisms of exosomal non-coding RNAs in human health and diseases. *Signal Transduct Target Ther.* 2021;6(1):383.
41. Henrich SE, McMahon KM, Plebanek MP, Calvert AE, Feliciano TJ, Parrish S, et al. Prostate cancer extracellular vesicles mediate intercellular communication with bone marrow cells and promote metastasis in a cholesterol-dependent manner. *J Extracell Vesicles.* 2020;10(2):e12042.
42. LA OR, Tai L, Lee L, Kruse EA, Grabow S, Fairlie WD, et al. Membrane-bound Fas ligand only is essential for Fas-induced apoptosis. *Nature.* 2009;461(7264):659–63.
43. Lu T, Zhang Z, Zhang J, Pan X, Zhu X, Wang X, et al. CD73 in small extracellular vesicles derived from HNSCC defines tumour-associated immunosuppression mediated by macrophages in the microenvironment. *J Extracell Vesicles.* 2022;11(5):e12218.
44. Deaglio S, Dwyer KM, Gao W, Friedman D, Usheva A, Erat A, et al. Adenosine generation catalyzed by CD39 and CD73 expressed on regulatory T cells mediates immune suppression. *J Exp Med.* 2007;204(6):1257–65.
45. Simoni Y, Becht E, Fehlings M, Loh CY, Koo SL, Teng KWW, et al. Bystander CD8(+) T cells are abundant and phenotypically distinct in human tumour infiltrates. *Nature.* 2018;557(7706):575–9.

Publisher's note

Springer Nature remains neutral with regard to jurisdictional claims in published maps and institutional affiliations.